Int J Earth Sci (Geol Rundsch) (2016) 105:1761–1778
DOI 10.1007/s00531-015-1174-2

ORIGINAL PAPER

Shaping the Rwenzoris: balancing uplift, erosion, and glaciation

Georg Kaufmann[1] · **Matthias Hinderer**[2] · **Douchko Romanov**[1]

Received: 29 November 2013 / Accepted: 29 March 2015 / Published online: 14 April 2015

Abstract The Rwenzori Mountains in Africa represent an extremely uplifted basement fault block at the eastern edge of the western branch of the East African Rift system, a large-scale rift system controlled by extensional stresses. The rugged alpine topography reaches an altitude of up to 5109 m, and the highest parts are ice-covered. Glacial landforms and moraines proof repeated more extensive glaciations during the last glacial cycles. In order to elucidate magnitudes and the varying role of erosional processes in shaping the relief of the Rwenzori Mountains over the past 2 mill. years, we performed numerical simulations with the landscape evolution programme ULTIMA THULE. It is controlled by a climate driver with temperature as a master variable as well as changing precipitation and evapotranspiration over time. The morphological processes considered are fluvial erosion, hillslope diffusion, and glacial abrasion, and the latter controlled by the simulated glaciation of the landscape. We provide three sets of model runs: the first one starting from the present-day topography and running for approx. 800 ka, the second one extending the modelling period to 2 Ma, and the third one starting from a peneplain and evolving for 2 Ma. Our results provide constraints on the temperature history of the Rwenzori Mountains, the interplay of morphological degradation and tectonic uplift, and a time frame for the formation of the mountain chain from a peneplain to the present relief. The modelled landscape evolves from a peneplain 2 Ma ago to a Rwenzori-type mountain range, when the fairly strong average rock uplift of 1–2 mm year^{-1} is compensated by a strong fluvial erosion component. The rock uplift rate is needed to obtain elevations above the equilibrium line altitude around 500 ka BP and results in surface uplift over time. Around that time, a periodic ice cap appears in the models, and glacial abrasion then limits the height of the Rwenzori Mountains to its present elevation.

Keywords Rwenzori Mountains · Geomorphology · Modelling

Introduction

In Africa, high-mountain topography (Fig. 1) with peaks reaching the 5000-m mark above sea level is limited to the Kilimanjaro (5895 m), the Mount Kenya (5199 m), and the Rwenzori Mountains (Margherita Peak, 5109 m). Of these three ranges, the Kilimanjaro and Mount Kenya are active volcanoes, while the Rwenzori Mountains represent an uplifted basement block located within the East African Rift system (EARS).

The formation of the EARS as a major plate-tectonic structure did not start before the late Palaeogene and is still active today. The EARS can be subdivided into the western branch and the eastern branch with the Nubian Plate in the west and the Somalian Plate in the east (Ebinger 1989; Ring 1993, 2008). In between the two branches, the mechanically strong Tanzania Craton is located (Fig. 1a). Along these branches, rift basins of around 60–90 km length and 50 km width have evolved, which are half-graben structures. The Moho is generally in about 30–35 km depth, raising to only 25 km depth below the rifts, and

✉ Georg Kaufmann
georg.kaufmann@fu-berlin.de

[1] Institut für Geologische Wissenschaften, Freie Universität Berlin, Malteserstr. 74-100, Haus D, 12249 Berlin, Germany

[2] Institut für Angewandte Geowissenschaften, Technische Universität Darmstadt, Schnittspahnstr. 9, 64287 Darmstadt, Germany

lithospheric thickness is around 125 km (Ritsema et al. 1999; Wölbern et al. 2010; Link et al. 2010; Lindenfeld et al. 2012).

The eastern branch stretches from the Afar triangle through Ethiopia and Kenya towards Tanzania, and it is characterised by active volcanism. Both Kilimanjaro and Mount Kenya are located on the rift shoulder of the eastern branch (Fig. 1), and the eastern rift itself is located in about 2000 m height above sea level (Ebinger and Sleep 1998; Morley 1999).

The western branch follows the western border of Uganda, Ruanda, Burundi, and Tanzania, and joins the eastern branch further south in Malawi (Fig. 1). Rifting started in the Miocene (Ebinger 1989; Bauer et al. 2010). The western branch has a higher seismicity than the eastern branch, with the Rwenzori region being the area with the highest seismicity (Lindenfeld et al. 2012). Volcanic activity in the western branch is limited (e.g. Virunga), but south and east of the Rwenzori Mountains some volcanic centres are developed (Toro-Ankole, Foley et al. 2012). The rift floors are covered by a series of lakes (from north to south Lake Albert, Lake George, Lake Edward, Lake Kivu, Lake Tanganyika , Lake Malawi).

Besides the steep rift flanks characteristic for the western branch, the Rwenzori Mountains are a very pronounced horst structure still connected to the eastern rift shoulder and rising more than 4 km above the rift floor, challenging to explain within the extensional setting of the EARS.

In this paper, we investigate and discuss the interaction of rock uplift of the Rwenzori Mountains and the morphological processes shaping the landscape. We employ the numerical landscape evolution model ULTIMA THULE (Kaufmann 2010), which simulates the effect of hillslope degradation, fluvial erosion, and glacial abrasion and is driven by climate boundary conditions (temperature, precipitation, and relief). We have already used this model in an earlier study (Kaufmann and Romanov 2012) to determine the required temperature drop to glaciate the Rwenzori Mountains as observed from field evidence and to estimate the rock uplift range needed to compensate for the morphological degradation of the surface.

We have organised the paper as follows: in section "Rwenzori Mountains", the Rwenzori Mountains are discussed, with special emphasis to the glaciation history derived from field evidence. In section "Numerical model", the landscape evolution model ULTIMA THULE is described, and the relevant processes are introduced and discussed. In section "Results", we present the results of our numerical analysis, subdivided into three scenarios: (1) estimate of temperature drop during peak glacial phases, based on model runs (800 ka run time, present topography) driven by a scaled stack of the marine oxygen-isotope record derived from benthic foraminifera (Lisiecki and Raymo 2005). (2) Extension of model back to 2 Ma to test a quasi-steady-state balance between uplift of the Rwenzori Mountains and river incision (2 Ma, present topography). (3) Model run based on an initial peneplain topography at 2 Ma experiencing uplift as a horst block bounded by faults and reaching a height of around 5 km.

Rwenzori Mountains

Geology and morphology

The Rwenzori Mountains horst structure is about 50 × 120 km in size, located just north of the equator and surrounded by Lake Albert to the north and Lake George and Lake Edward to the south. Towards the rift in the west, the Rwenzori block is separated through the Bwamba fault and almost separated from the rift shoulder through the Rwimi–Wasa fault and the Nyamwamba fault in the east (Fig. 2). The Rwenzori block itself is composed of Archean gneisses and palaeoproterozoic metavolcanic and metasedimentary rocks (amphibolites, micashists, quartzites) (see Bauer et al. 2012, for a review), whereas the rift is filled with up to 4-km-thick fluvial and lacustrine sediments (Pickford et al. 1993; Roller et al. 2010). In the Edward rift to the south, quaternary pyroclastic rocks contribute to the rift fill and led to widespread volcanic cover of the syn-rift sediments (Koehn et al. 2010).

Basement rocks in the region show a displacement at the border faults of up to 8 km (Ring 2008), i.e. an extreme topographic gradient is tectonically induced. Hence, the topography of the mountain chain is very pronounced, with steep valleys and clear glacial landforms in the higher alpine area. The highest elevation is Margherita Peak (5109 m) on the border of the Democratic Republic of Congo and Uganda, and the foothills are located in around 1000 m elevation, and the rift floor at around 700 m (Fig. 2). The dissection of the horst is mainly controlled by large normal faults in N–S, NW–SE, and E–W directions, and some of the faults have a significant strike-slip component (Ring 2008; Koehn et al. 2010).

Valleys are usually steep and show V-shaped sections with very little sediment accumulation. In the glaciated central Rwenzori Mountains, however, also U-shaped valleys are present bearing some fluvio-glacial and glacial sediments together with rock fall deposits and well-preserved moraine ridges and glacial lakes (Osmaston 1989). The hillslopes and valleys are covered by dense tropical vegetation which suppresses erosional processes at least since the Holocene (Roller et al. 2012). Only in regions higher than 4000 m, bare rock surfaces and glaciers offer a stronger erosional regime. Roller et al. (2012) determined erosion rates between 28 and 131 mm ka^{-1}, using

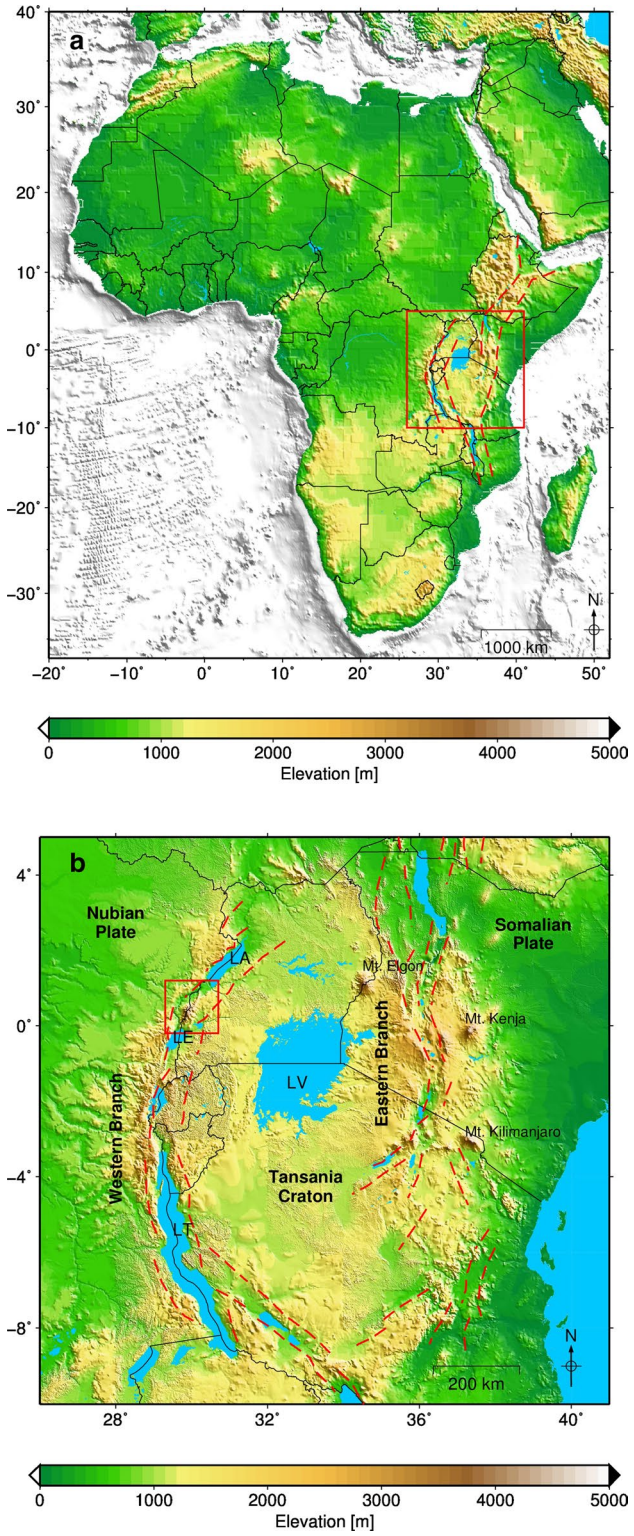

Fig. 1 Topography and tectonic structure of East Africa. **a** Overview of Africa, with the research area enclosed by *red line*. **b** East African Rift system, with the western and the eastern branch, the Nubian and Somalian Plates, and the Tanzania Craton in between. Major faults are shown as dashed lines, and the *rectangle marks* the area shown in Fig. 2. *LV* Lake Victoria, *LT* Lake Tanganyika, *LA* Lake Albert, *LE* Lake Edward. Topography data from shuttle radar topography mission (SRTM, Farr et al. 2007)

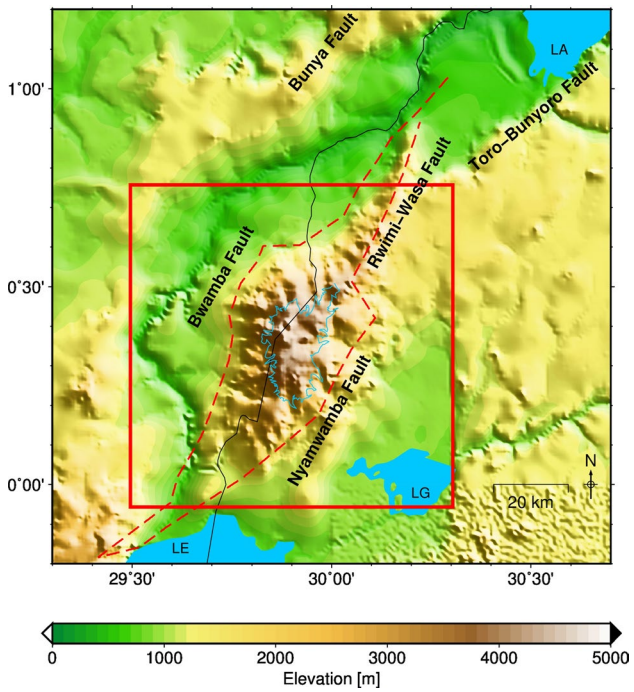

Fig. 2 Topography and simplified tectonic structure of Rwenzori Mountains, with major faults shown as *dashed red lines*. The *blue line* is the estimated glacial cover at the last glacial maximum, and the *red line* indicates the model area chosen for numerical simulations. *LV* Lake Victoria, *LT* Lake Tanganyika, *LA* Lake Albert, *LG* Lake George, *LE* Lake Edward. Topography data from SRTM (shuttle radar topography mission, Farr et al. 2007)

cosmogenic nuclides surpassing those of the rift shoulder by about one order of magnitude. Nevertheless, these rates are low compared to compressional mountain ranges with similar topography.

The evolution of the western branch and the Rwenzori Mountains is not clearly understood yet (e.g. Pickford 1990; Van Damme and Pickford 2003), but several stages can be identified (see Bauer et al. 2010, 2013, and references therein): (1) 20–18 Ma: early faulting and subsidence of Albertine section of western branch of the EARS. (2) 12 Ma: initial volcanic activity in Virunga Province and early sedimentation in the Albertine Rift. (3) 10–8 Ma: tectonic movements in Lake Albert and Lake Kivu areas. (4) 8.5–8 Ma: first major rifting episode in Lake Albert area with rift-flank uplift. (5) 7.5–2.5 Ma: large palaeolake (Lake Obweruka) covered rift from (present) Lake Albert to (present) Lake Edward. (6) 3–2 Ma: second tectonic pulse in Lake Albert area, initiation of strong uplift of the Rwenzori fault block.

Climate

The Rwenzori Mountains are located close to the equator; thus, the innertropical convergence zone moves over the

area twice a year. Rain seasons are from March to May and from September to December; the rest of the year is rather dry in the lowlands (Osmaston 1989). At higher altitudes, however, moisture and rain are abundant year-round, as the high-mountain topography of the Rwenzori Mountains disturbs the atmospheric circulation and attracts a permanent cloud cover (Kappelle 2004).

Precipitation is strongly altitude dependent: from 1000 to 2000 m altitude, it increases from 500 to 2500 mm year^{-1}, peaking in around 3500 m, then decreasing to 2000 mm year^{-1} in higher altitudes (Osmaston 1989). Additionally, there is a strong fluctuation in palaeoprecipitation observed in Eastern Africa: north of the Rwenzori Mountains in the Lake Albert region, Beuning et al. (1997) found evidence of lower lake levels of Lake Albert for the period between 30 and 18 ka BP, with the lowest lake level around 18 ka BP. This low lake levels indicate drier climatic conditions, when compared to the present. Bonnefille and Chalie (2000) sampled peat bogs between 2° and 4°S in Ruanda and analysed their pollen spectra. From these data, they estimate a reduction of palaeoprecipitation of about 30 % during the last glacial maximum (LGM) relative to the present. Felton et al. (2007) confirmed results from Bonnefille and Chalie (2000), analysing a sediment core from Lake Tanganyika. The core covers about 60 ka of time and reveals a drier period between 32 and 18 ka BP, both preceded and followed by wetter periods such as the present period. On the eastern branch of the EARS, Barker et al. (2011) sampled a sediment core from Lake Challa on the slopes of Mount Kilimanjaro and retrieved a 25-ka-long record, also indicating drier conditions during the LGM. Thus, the reduction of palaeoprecipitation in Eastern Africa around 30–20 ka BP is a regional phenomenon. Palaeoclimate records older than the LGM are scarce (e.g. Gasse 2000). Scholz et al. (2007) found episodes of extreme lake level lowering and thus extreme dry periods ("mega droughts") between 135 and 75 ka BP from scientific drill cores on Lake Malawi coincident with enhanced orbital eccentricity and precession. After 70 ka, the region shifted to more stable humid conditions with diminished climate extremes. Extreme unstable and fluctuating climate conditions during this time are also reported from the eastern branch of the EARS (Trauth et al. 2003). The dominance of superimposed eccentricity and precessional orbital signals is valid at least for the past 3 Ma and dominates the tropical African hydrological cycle by changes of low-latitude heating via its impact on monsoon dynamics as has been shown by Trauth et al. (2003) based on marine and continental climate records. However, results from climate circulation models (Kaspar et al. 2010; Prömmel et al. 2013) suggest that the development of the EARS and the emergence of the Rwenzori Mountains decreased precipitation west of the EARS, but increased precipitation east of the EARS.

Glaciation

Ice coverage of the Rwenzori Mountains has been very variable during the quaternary, with larger ice caps present during peak glacial phases (see Osmaston and Harrison 2005, for a review). Except for a radiocarbon age from sediments of a kettle hole of the Lake Mahoma stage, linking it with the Last Glacial Maximum in high latitudes, the chronology of glacial stages in the Rwenzori Mountains is only based on field observations of the freshness of glacial landforms and geomorphological consideration of dissection of older glacial stages (Osmaston 1989). Hence, dating of glacial stages is still tentative. A new glacial chronology for equatorial East Africa has been developed by Shanahan and Zreda (2000) using in situ cosmogenic ^{36}Cl measured in 122 boulders from moraines on Mount Kenya and Kilimanjaro.

The earliest phase in the Rwenzori Mountains was the Katabarua Glaciation, whose moraines are thought to be older than 300 ka BP. This stage or stages might be synchronous to the Liki I stage at Mount Kilimanjaro and Mount Kenya dated to 355–420 ka BP (Shanahan and Zreda 2000). From the locations of the moraines and tills associated with the Katabarua Glaciation, a large ice cap of around 500 km^2 has been deduced, the largest glaciation of the Rwenzori Mountains. The subsequent Rwimi Glaciation is estimated to an age of at minimum 100 ka BP and might be linked to the Teleki stage between 255 and 285 ka according to cosmogenic dating of boulders at Mount Kilimanjaro and Mount Kenya (Shanahan and Zreda 2000). The ice cap was slightly smaller, around 300 km^2 in size, but the glaciers progressed to lower altitudes in the steep valleys. There seems to be no glacier advance at MIS (Marine Isotope Stage) 6 (ca. 130 ka BP), maybe due to severe dry conditions at this time.

The Lake Mahoma Glaciation, coinciding with the LGM, has well-preserved moraines, from which the character of the ice cap at the LGM can be deduced (Fig. 2): a group of ice caps is covering the six main peaks (around 260 km^2), which were drained by deep glacial valleys descending down to 2000–2400 m. The reconstruction of the equilibrium line altitude (ELA) results in a slightly tilted, elongated LGM ice cap following the general relief of the mountains and the predominant wind direction (Osmaston and Harrison 2005). The Lake Mahoma stage can be correlated with the Liki II moraines at Mount Kenya and moraines of the fourth Glaciation on Mount Kilimanjaro where they give ages between approx. 28 and 20 ka, respectively.

Two later glaciations, the Omurubaho Glaciation (estimated to 10 ka BP, 70 km^2) and the Lake Gris Glaciation (estimated to 3 ka BP, 10 km^2) mark temporal readvances after the LGM also known from Mount Kilimanjaro and Mount Kenya (Shanahan and Zreda 2000). The Omurubaho stage might be linked to some temperature drop during the Younger Dryas and general more humid conditions compared to the LGM as known from lake records (e.g. Beuning et al. 1997).

Today, the highest peaks are still permanently snow covered. In 1906, glaciers covered around 7.5 km^2, at that time half of the total glacier area in Africa. Modern glaciers, however, are fairly small, covering 1.7 km^2 around 1990 (Kaser 2001), and shrinking to 1.5 km^2 by 1995 (Osmaston and Harrison 2005), and below 0.5 km^2 at present.

Numerical model

Landscape degradation following morphological processes such as hillslope diffusion, fluvial erosion, glacial abrasion, rock uplift, and isostatic response is modelled with the numerical landscape evolution model ULTIMA THULE. The model is based on a regular grid, on which the relief $h(x, y, t)$ (m) is described as a function of space and time, with x (m) and y (m) the eastward and northward coordinates, and t (s) the time. The relief $h(x, y, t)$ (m) is the sum of bedrock topography $h_\mathrm{B}(x, y, t)$ (m), sediment thickness $h_\mathrm{S}(x, y, t)$ (m), ice thickness $h_\mathrm{I}(x, y, t)$ (m), and vertical flexural-isostatic displacement $h_\mathrm{F}(x, y, t)$ (m). The change in relief, surface uplift, and/or peneplanation is the sum of the individual contributions (rock uplift, hillslope diffusion, fluvial erosion, glacial abrasion, isostatic flexure):

$$\begin{aligned}\frac{\mathrm{d}h(x,y,t)}{\mathrm{d}t} = &\left(\frac{\partial h(x,y,t)}{\partial t}\right)_{\text{uplift}} + \left(\frac{\partial h(x,y,t)}{\partial t}\right)_{\text{hillslope}} \\ &+ \left(\frac{\partial h(x,y,t)}{\partial t}\right)_{\text{fluvial}} + \left(\frac{\partial h(x,y,t)}{\partial t}\right)_{\text{glacial}} \\ &+ \left(\frac{\partial h(x,y,t)}{\partial t}\right)_{\text{flexure}} \qquad (1)\end{aligned}$$

The individual morphological processes are applied sequentially during a numerical timestep, but are coupled beyond that numerical timescale via their contributions.

The numerical model predicts changes in the relief according to (1) as well as the movement of sediment, ice, and water through the landscape. All model parameter values, and their respective standard values, are listed in Table 1. The different processes will be shortly discussed next; however, a more detailed mathematical description of ULTIMA THULE can be found in Kaufmann and Romanov (2012).

Table 1 Variables and reference model parameters

Description	Symbol	Unit	Value
Eastern coordinate	x	m	Input parameter
Northern coordinate	y	m	Input parameter
Time	t	s	Input parameter
Grav. acceleration	g	m s^{-2}	9.81
Relief			
Relief height	h	m	Calculated
Bedrock height	h_B	m	Calculated
Sediment thickness	h_S	m	Calculated
Ice thickness	h_I	m	Calculated
Slope	s	–	Calculated
Ice sheet			
Density of ice	ρ_I	kg m^{-3}	910
Ice-deformation coefficient	A_D	m^6 year^{-1} N^{-3}	2.5×10^{-16}
Ice-sliding coefficient	A_S	m^7 year^{-1} N^{-3}	1.9×10^{-10}
Ice exponent	n	-	3
Abrasion parameter	κ_I	m^2 s^{-1}	Calculated
Hillslope processes			
Diffusion coefficient (bedrock)	κ'_D	m^2 year^{-1}	0–1.5
Diffusion coefficient (sediment)	κ'_D	m^2 year^{-1}	$10 \times \kappa'_D$ for bedrock
Diffusion coefficient (ice)	κ'_D	m^2 year^{-1}	0
Critical slope	s_crit	–	1
Fluvial processes			
Precipitation	N	m s^{-1}	Input parameter
Temperature	T	°C	Input parameter
Evapotranspiration	ET	m s^{-1}	Calculated
Runoff	q	m^3 s^{-1}	Calculated
Sediment load	Q	m^{-3} s^{-1}	Calculated
Carrying capacity	Q_e	m^3 s^{-1}	Calculated
Erosion coefficient	κ_R	–	0–0.01
Channel width	w	m	Calculated
Channel coefficient	w_r	s$^{0.5}$ m$^{-0.5}$	0.1
Length scale (bedrock)	L	m	100×10^3
Length scale (sediment)	L	m	10×10^3
Glacial processes			
Abrasion coefficient	k_C	m^{1-m} s^{m-1}	0–0.01
Abrasion exponent	m	–	1
Valley constriction	β	–	Calculated
Constriction coefficient	k_C	m	1000
Isostatic processes			
Density of crust	ρ_C	kg m^{-3}	2500
Density of mantle	ρ_M	kg m^{-3}	3000
Density of sediment	ρ_S	kg m^{-3}	1500
Thickness of elastic plate	h_plate	m	30×10^3
Shear modulus	μ	Pa	6.7×10^{10}
Poisson's ratio	ν	–	0.25

Tectonic processes

The cause of the extreme uplift of the Rwenzori Mountains is still debated in the literature. While Wallner and Schmeling (2010, 2011) favour the delamination of a part of the mantle lithosphere, which then causes a rebound of the crust due to the missing weight of the detached lithospheric root, Sachau and Koehn (2010) and Sachau et al. (2013) argue that fault evolution in the stiff crust in an extensional setting causes strong localised rock uplift, which can explain the amount of surface uplift of the Rwenzori block. In our numerical model, we simply assign an external uplift function with an uplift velocity $U(x, y, t)$ (m s^{-1}). It corresponds to the rock uplift independently of driving tectonic or mantle processes. Thus, rock uplift in our model is not taken into account as tectonic process, but as mathematical function with pre-defined uplift rate.

Hillslope processes

Weathering, rock and mud slides, and soil creep are oriented downwards and are proportional to local slope. Thus, they can be modelled by a mass flux (regolith layer thickness times sliding velocity). Mass conservation is then applied by modelling the flux derivatives within a diffusion equation (e.g. Beaumont et al. 1992; Kooi and Beaumont 1994; Tucker and Slingerland 1994; Braun and Sambridge 1997). For bedrock, sediments, and ice-covered areas, we assign different diffusion coefficients (see Table 1).

Fluvial processes

The surface runoff as the difference between precipitation and evapotranspiration follows the steepest gradient in hilly landscapes, and runoff quickly converges to form trickles, creeks, and rivers. Within these runoff channels, material can be removed by erosion or deposited from the creeks and rivers, when local slope becomes smaller and thus runoff velocities decrease. We employ the CASCADE algorithm (Braun and Sambridge 1997; Braun and Willet 2013), which allows for an explicit calculation of the sediment load suspended in the water. However, we stress that the parameterisation of river incision is still debated in the literature (e.g. Kooi and Beaumont 1994; van der Beek and Bishop 2003). We therefore test different river erosion coefficients to bracket possible rock types.

Glacial processes

If the temperature is below the freezing point, surface runoff stops and snow is accumulated. For prolonged periods of snow fall, snow is compressed and eventually transformed to ice, which builds up glaciers and ice caps. The ice cover is modelled with the shallow ice approximation; thus, the ice velocities must be small when compared to the vertical derivatives (e.g. Hutter 1983). If ice velocities become too large, e.g. in constricted valleys, a numerical correction is applied (e.g. Braun et al. 1999; Tomkin and Braun 2002; Tomkin 2009). If the ice cover can move along the bedrock surface, glacial abrasion occurs. In our numerical model, we employ a simple relation describing glacial abrasion, relating the abrasion to the basal velocity of the ice stream (Hallet 1979; Braun et al. 1999; Tomkin and Braun 2002; Tomkin 2009). This should well reflect warm-based conditions of tropical glaciers.

Isostatic processes

The reaction of the lithosphere and the asthenosphere to the changing relief is modelled by a thin elastic plate overlying a viscous substratum (Turcotte and Schubert 1982).

Climate

Landscape evolution of the Rwenzori Mountains as discussed by our numerical model ULTIMA THULE is driven by climatic variability. Surface temperature, precipitation, and other climate parameter vary on all timescales. We account for this variability by using a present temperature distribution $T_0(x, y)$ (°C) fixed at sea level and accounting for the relief with an elevation-dependent adiabatic lapse rate α (°C km^{-1}).

Palaeotemperatures $T(x, y, t)$ are then derived according to

$$T(x, y, t) = T_0(x, y) + \alpha h(x, y, t) + GI(t)\Delta T. \quad (2)$$

The last term on the right-hand side accounts for the temporal variation using a temperature offset ΔT (°C) and a glacial index function $GI(t)$, which is normalised such that $GI(t) = 0$ holds for interglacials, and $GI(t) = 1$ for the LGM.

The glacial index function can be based on a palaeoclimate archive, such as an ice core or a sediment record, which are a proxy of temperature. In Kaufmann and Romanov (2012), we used the hydrogen-isotope record measured in the Dome C Antarctic ice core (EPICA 2004, black line in Fig. 3) to derive a glacial index function. In this paper, we employ the benthic foraminiferal record from a stack of deep-sea sediment cores (Lisiecki and Raymo 2005, red line in Fig. 3), which bears more relation to the African climate variability than the Antarctic Dome C record. We note, however, that the temporal variability described by both palaeotemperature archives is fairly similar: the periodicity of the glacial cycles is almost identical,

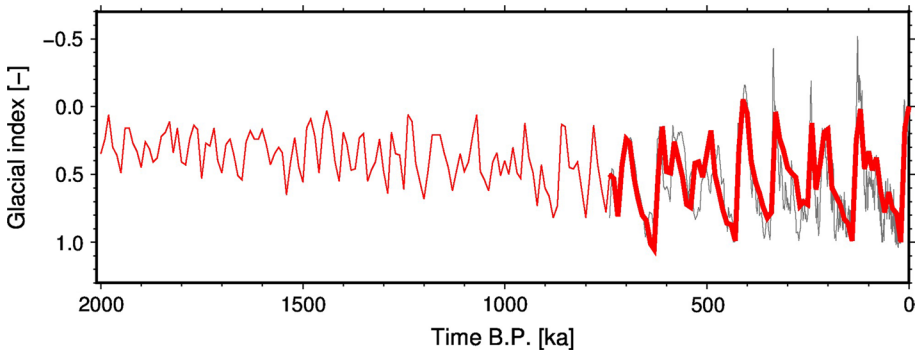

Fig. 3 Glacial index (*GI*) as a function of time before present (BP). The variation is derived from the oxygen-isotope record of benthic foraminifera from different ocean sediment cores (Lisiecki and Raymo 2005, *red lines*, *thick red line* used for setup 1), and the hydrogen-isotope record of the Dome C Antarctic ice-core record (Petit et al. 1999, *black line*). The isotope records have been scaled to the present ($GI = 0$) and the last glacial maximum ($GI = 1$)

but the ice-core record has a distinct high-frequency signal due to the denser sampling of the ice-core archive with respect to the deep-sea sediment cores. Thus, our new climate driver derived from the benthic foraminifera record essentially is a smoothed glacial index function, when compared to the ice-core record.

Surface runoff $R(x, y, t)$ (m s^{-1}) is based on the following equation:

$$R(x, y, t) = N_0(x, y) - ET(x, y, t) + NI(t)\Delta N. \quad (3)$$

Here, present precipitation $N_0(x, y)$ (m s^{-1}) is fixed to 2500 mm year^{-1}, the observational value derived for 2000–4000 m elevation in the Rwenzori Mountains (Osmaston and Harrison 2005). The temporal variability is controlled by two processes: on the one hand, variable evapotranspiration $ET(x, y, t)$ (m s^{-1}), which depends on temperature $T(x, y, t)$, and thus on time; on the other hand, on temporal variations in the palaeoprecipitation itself, which is described by a precipitation index function $NI(t)$ (in analogy to the glacial index function) and a precipitation offset ΔN, the difference between present precipitation and the LGM. As we have only field evidence on changes in precipitation back to 40 ka BP, we used $NI(t) = 0$ for our model runs. Thus, we overestimate the palaeoprecipitation, but this has only a minor influence on ice-sheet evolution, as temperature control is supposed to be more important in the high-mountain climate of the Rwenzori Mountains (Taylor et al. 2006). We can also argue that the Rwenzori Mountains as a high-mountain relief experienced less variability in precipitation, as they act as a large barrier capturing precipitation (e.g. Osmaston 1989).

Parameterisation of the ice mass balance follows a simple temperature relation (e.g. Tomkin and Braun 2002; Tomkin 2003, 2007). For more details, concerning the numerical implementation the reader is referred to (Kaufmann and Romanov 2012).

Results

In this section, we present and discuss the results of our numerical simulation of the interaction of palaeoclimate variability, morphological processes, and rock uplift of the Rwenzori Mountains. We have subdivided the section into three parts:

1. We first run models for approx. 800 ka and start with the present-day topography. This part repeats results from Kaufmann and Romanov (2012), but with a different glacial index function (deep-sea sediment records instead of ice record). With this modification, we want to analyse the effect of different climate drivers on the evolving landscape.
2. In the second part, we extent the period modelled to 2 Ma, but retain the present-day topography as start model. We intent to figure out, if the quasi-steady state obtained in the first set of model runs is stable over longer periods.
3. In the last part, we keep the longer 2-Ma run time, but our initial topography now is a peneplain, and the region of the Rwenzori bounded by the three important normal faults (Fig. 2) will uplift with a pre-defined rock uplift rate. With this set of model runs, we want to answer the question, whether a peneplain model will evolve into a "Rwenzori-style" mountain chain.

We base the first two sets of models on a topography derived from the Shuttle Radar Topography Mission (SRTM, Jarvis et al. 2008), with a discretisation into surface elements 250 × 250 m in size. The model region is 90 × 90 km wide. The present-day equilibrium line is located in around 5000 m height, the equilibrium line at peak glacial times in around 3900–4000 m, increasing the area of potential ice growth. Time steps for the numerical

model are variable, depending on ice coverage: if no ice is present, the model advances with time steps of 100 years, but when an ice cover is present, the time steps are dynamically reduced to allow convergence of the shallow ice-sheet equation. Morphological parameter values (see Table 1) are identical to the ones used in Kaufmann and Romanov (2012), but the glacial index function is based on the deep-sea oxygen stack (see section "Climate"). For the entire model, the parameter values for erosion, hillslope diffusion, and glacial abrasion are fixed, thus describing a homogeneous lithology. As this assumption is clearly wrong, we have explored the dependence of the model results on the hillslope, the fluvial, and the glacial diffusion coefficient in Kaufmann and Romanov (2012), and from this sensitivity analysis, we concluded that rock strength affects the evolution by <20–30 %. Furthermore, we simplified the uplift of the Rwenzori Mountains to the uplift of a single block without considering differential uplift. Thermochronological studies revealed evidence that this assumption is not true for the long-term history of the Rwenzori Mountains (Bauer et al. 2010, 2013). However, it remains unclear from these data if and how differential uplift continued during the last 2 Ma. There is a clear offset between parameter values controlling erosion and rock uplift; weaker rock strength resulting in more degradation of the landscape needs to be compensated by higher uplift.

Setup 1: Present topography, 800 ka

In this first setup, we start each model with a discretised version of the present-day topography and run the model for 800 ka.

Setup1a We first estimate the temperature drop ΔT needed to produce a glacial coverage at around 25 ka BP similar to the observed Lake Mahoma glaciation (Fig. 2). For temperature drops between $\Delta T \in [-4.5; -6.5]$ °C, ice caps periodically cover the higher alpine area of the Rwenzori Mountains, with the largest cover between 100 and 400 km^2 during peak glacial phases. However, a temperature drop of $\Delta T = -6.5$ °C (blue areas) is needed to reproduce the extent of the Lake Mahoma glacial phase, as it can be seen in the ice extent shown in Fig. 4a. This result is in agreement with the inference from Kaufmann and Romanov (2012), based on the glacial index derived from the hydrogen-isotope record of the Antarctic Dome C ice core.

Setup1b In the next step, we activate hillslope diffusion, fluvial erosion, and glacial abrasion as morphological processes. We vary the controlling parameter values within large bounds: for hillslope diffusion between $\kappa_D \in [0.7, 1.5]$ m^2 year^{-1}, for fluvial erosion between $\kappa_R \in [0.001, 0.01]$, and for glacial abrasion between $\kappa_G \in [0.0001, 0.01]$. We have chosen the parameter space for the three morphological processes in accordance with other literature sources (e.g. Herman and Braun 2008; Tomkin 2009), but we admit that the scarcity of robust field evidence does not allow us to properly limit the parameter values. Still, the parameter variation covers a wide range of rock types, from sedimentary rocks to metamorphic rocks.

The results are again in close agreement with Kaufmann and Romanov (2012), and our conclusions of the sensitivity analysis of the morphological parameter values based on Fig. 7 of Kaufmann and Romanov (2012) remain valid: increasing the strength of hillslope diffusion will remove more material from the slopes; thus, the landscape elevation is reduced and less area is available for glaciation with time. Decreasing the strength of fluvial erosion, however, leaves more sediment in the valleys, as the sediment is not transported downstream, but now hillslope diffusion becomes stronger, as transport by diffusion is ten times more effective for sediments than for bedrock, and landscape elevation is again reduced. This is the reason for less ice cover, if fluvial erosion is weaker. Changing the strength of glacial abrasion does not have a significant effect on the landscape degradation, as the ice-covered area is too small in the case of the Rwenzori Mountains.

We now progress with a typical model to evaluate the ice cover. Here, we fixed the parameter values to $\kappa_D = 1.5$ m^2 year^{-1} for hillslope diffusion, $\kappa_R = 0.005$ for fluvial erosion, and $\kappa_G = 0.01$ for glacial abrasion. As expected, the morphological processes reduce the topography with time; thus, the high-mountain area available for glaciation reduces with increasing run time. This can be seen in the reduction in ice extent shown in Fig. 4a, where the ice cover (black areas) becomes smaller for the last glacial periods.

Setup1c In a last step, we add a rock uplift component of $U = 0.5$ mm year^{-1} to the previous model, while the other parameter values are as above. The rock uplift rate is largest in the centre of the Rwenzori Mountains and decreases to zero towards the foreland, following a smoothed version of the present-day topography. The ice cover for this run is again shown in Fig. 4a.

As already inferred in Kaufmann and Romanov (2012), the uplift compensates the degradation of the surface by morphological processes, and ice cover (red solid line) is again able to explain the Lake Mahoma glaciation, producing a similar ice coverage as in the first run.

We can quantify the strength of the morphological processes by discussing the removal rates. We base this analysis on the last model of the previous discussion (setup1c), including an ice sheet, morphological processes, and rock uplift.

In Fig. 4b, the removal rates are shown for hillslope diffusion, fluvial incision, and glacial abrasion. For the chosen strength of the processes, both hillslope diffusion and

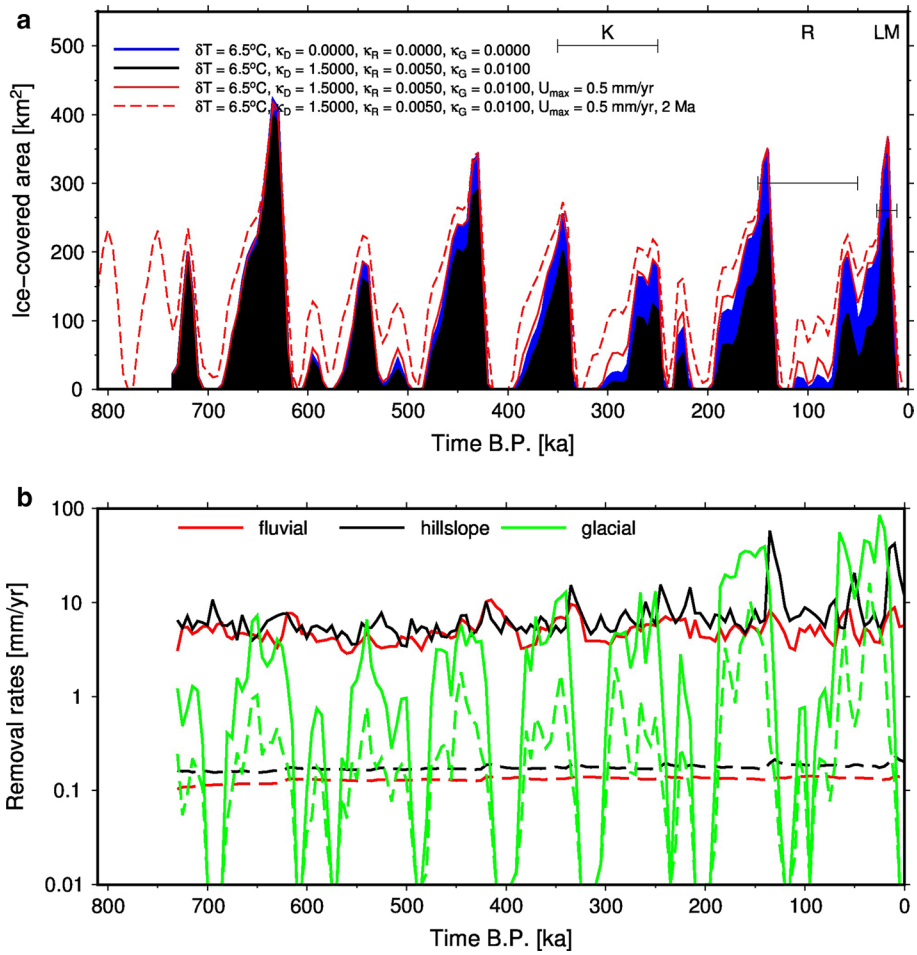

Fig. 4 Setup 1: **a** ice-covered area as a function of time BP. Lines resp. *coloured areas* represent runs with different parameters (see text). Also shown are the observed moraine-covered areas for the three different glaciations Katabarua (K), Rwimi (R), and Lake Mahoma (LM). **b** Removal rates for different processes (see legend). *Solid lines* indicate maximum rates, *dashed lines* average rates

fluvial incision have similar capacities to change the relief of the Rwenzori Mountains. The maximum removal rates close to 10 mm year^{-1} are a result of the steepness of the range. Average removal rates are, however, almost two orders of magnitude lower, thus more in accordance with global rates estimated for high tropical mountain ranges (e.g. Roller et al. 2012). Both the removal rates for hillslope diffusion and fluvial erosion show only moderate variations from the varying climate. The glacial removal rate, however, has a clear periodicity, resulting from the climate variability. In peak glacial periods, its maximum removal rate is as strong as the two other processes. The same holds true for the average removal rate for glacial abrasion, which, during cold spells, can be even higher than their counterparts hillslope diffusion and fluvial incision.

In Fig. 5, we discuss the individual contributions (ice sheet, morphological processes) for the LGM at around 25 ka BP. The ice cap covers the entire high-mountain area, as indicated by the observations of the Lake Mahoma glaciation (Osmaston 1989).

Fluvial incision is by nature of this process fairly widespread in the model domain. Removal of material in most cases focusses on steep valleys, with maximum incision of several hundred metres. The material is then transported downstream and deposited on the adjacent rift basins of the Rwenzori Mountains. On the eastern side, a large alluvial fan has been created in front of the Mobuku Valley, while on the western Congolese side the sediments have drowned the rift valley. Note that due to the limited extent of the model domain, the modelled Semliki River has no catchment and thus sediments are not correctly transported in the rift valley itself.

Hillslope diffusion has a clear bimodal pattern, with the removal of material along the steep ridges, and deposition near the flatter valley bottoms. However, most of the material stored in the high-mountain valleys by hillslope diffusion is then removed downhill by fluvial transport.

Glacial abrasion is limited to the top of the Rwenzori Mountains, with a clear preference of removal on the steep slopes of the mountain tops. Thus, the sliding ice is responsible for the oversteepening of slopes to form local cirques in the central Rwenzori Mountains. The total removal by glacial abrasion since roughly 800 ka BP considered approaches 100 m surface lowering.

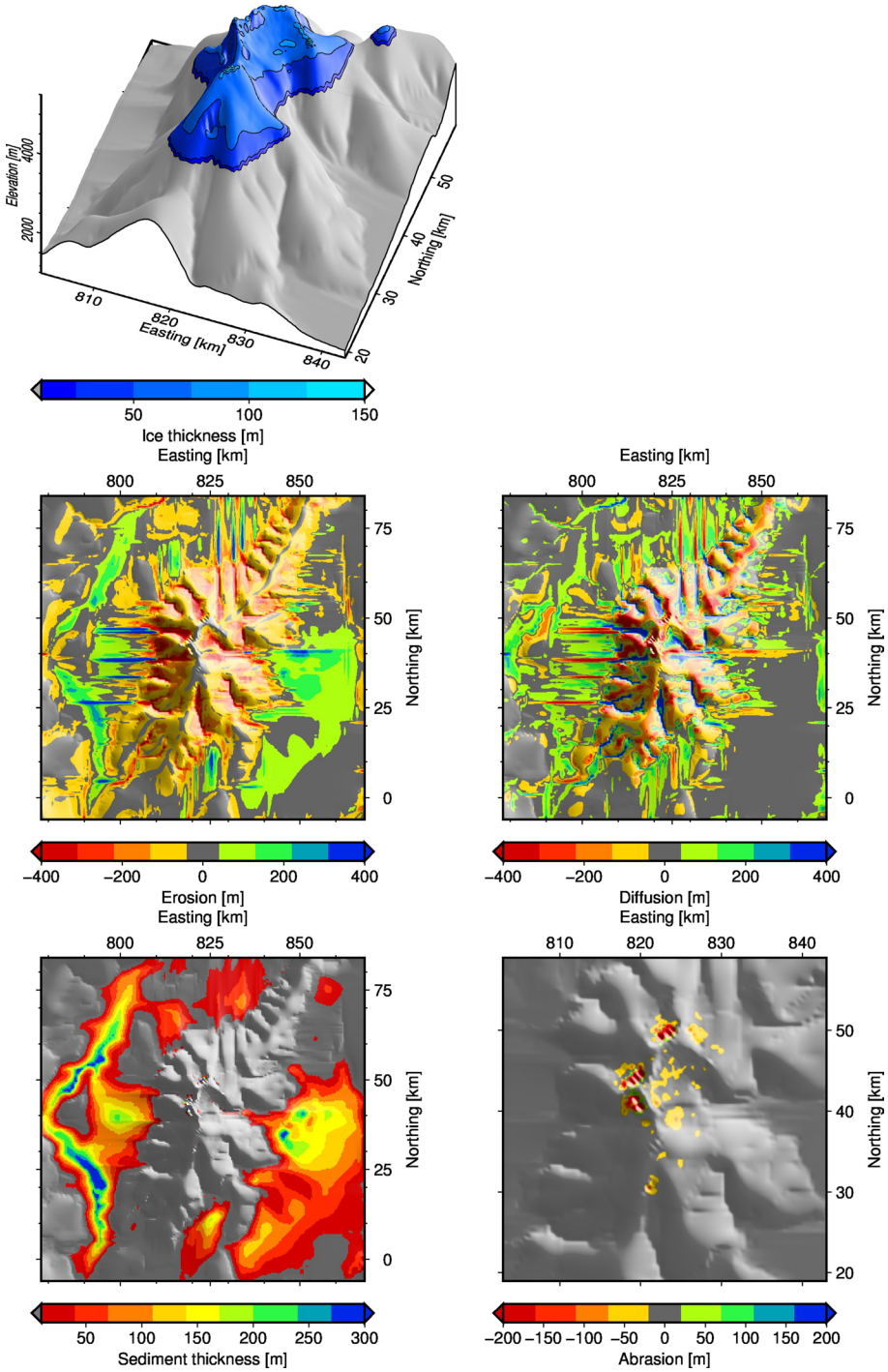

Fig. 5 Setup 1: morphological processes at 25 ka BP. Shown are the contributions from ice cover (*top left*), fluvial erosion (*middle left*), hillslope diffusion (*middle right*), sedimentation (*bottom left*), and glacial abrasion (*bottom right*). The latter four contributions are cumulative over 800 ka

Sedimentation occurs almost exclusively in the rift basins, with thick sediment infill both on the eastern and on the western side of the Rwenzori Mountains. Thicknesses of sediment accumulation in the rift basins are not appropriately modelled, e.g. fluvial distributary systems, lakes, and base-level changes have not been considered.

We conclude this part by highlighting the interaction of climate-driven, morphologically driven, and tectonically driven processes on the landscape evolution in the Rwenzori Mountains. In general, removing material by hillslope diffusion, fluvial incision, and glacial abrasion reduces topography and thus decreases the height over the equilibrium line. Ice sheets therefore become smaller with time due to the smaller accumulation area. Adding a rock uplift component to the model allows to compensate the degradation of the mountains by morphological processes, and a

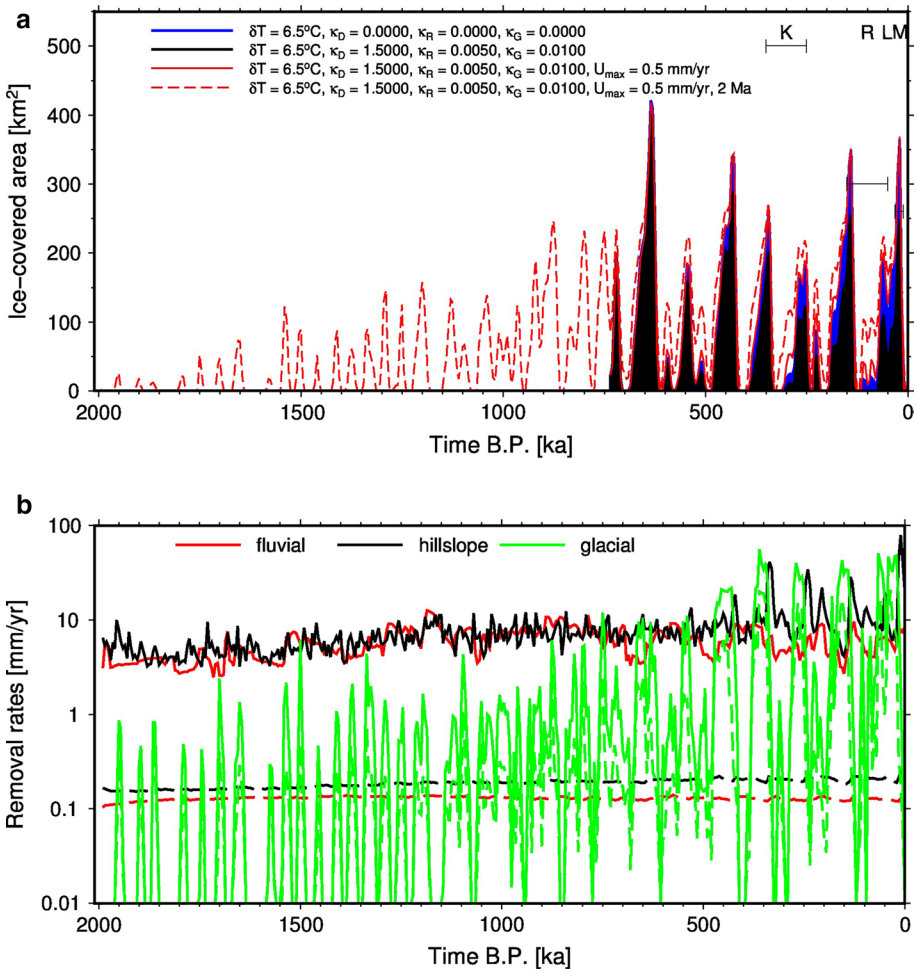

Fig. 6 Setup 2: **a** ice-covered area as a function of time BP. Lines resp. *coloured areas* represent runs with different parameters (see text). Also shown are the observed moraine-covered areas for the three different glaciations Katabarua (K), Rwimi (R), and Lake Mahoma (LM). **b** Removal rates for different processes (see legend). *Solid lines* indicate maximum rates, *dashed lines* average rates

quasi-steady state is kept, keeping the maximum elevation of the Rwenzori Mountains. We have also shown that the choice of the palaeoclimate archive used to derive the glacial index function is of minor importance, as long as the cyclicity of the ice ages is correctly parameterised.

Setup 2: Present topography, 2 Ma

In this section, we extent the model runs of the previous section to cover 2 Ma. We keep the present-day topography as starting model and drive the evolution with the glacial index function derived from the deep-sea sediment. We activate ice-sheet evolution, morphological processes, and rock uplift as in the last section (setup1c).

Setup2: In Fig. 6a, the ice cover for the 2-Ma run is shown as a function of time and compared to the runs from the previous section. Two important conclusions can be drawn from the result: firstly, the 2-Ma-long run (dashed red line) reproduces the cyclicity of the ice cover from the shorter 800-ka-long run (solid red line), and differences only arise within individual glacial cycles, but are minor. Secondly, the ice cover is significantly smaller further back in time, which is a result of smaller amplitudes of the glacial index before 1 Ma.

In Fig. 6b, the removal rates are shown for the 2-Ma-long run. Both the maximum fluvial and hillslope rates (solid red and black lines, respectively) are similar for the common 800 ka BP period. Before, also no fundamental change can be observed, except the slight reduction in amplitudes. The same holds for the average rates (dashed red and blue lines). The removal rate for glacial abrasion for times before 1 Ma, however, is at least one order of magnitude smaller than the corresponding fluvial and hillslope rates. Again, this is owed to the reduced amplitude of the glacial index function for these older times.

In summary, the extension of the modelling period from 800 ka to 2 Ma results in a similar evolution of the landscape, and again a *quasi-steady state* is kept, because rock uplift and erosional degradation are balanced, thus keeping the maximum elevation of the Rwenzori Mountains. Thus, this stationary feature, balancing rock uplift and morphological degradation, can be assumed to be a long-term effect.

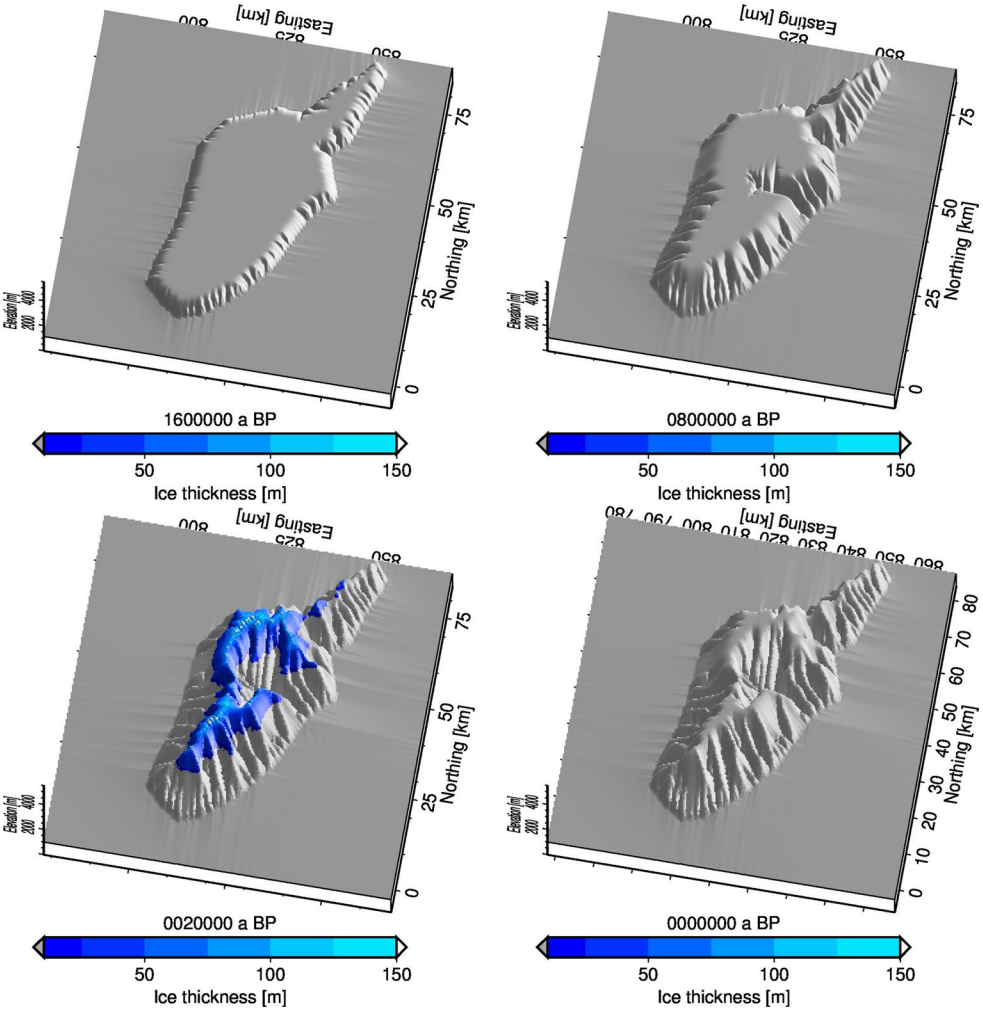

Fig. 7 Setup 3: morphology and ice cover for different times for the model starting from a peneplain topography and uplifting with $U = 1.8$ mm year^{-1}

Setup 3: Peneplain topography, 2 Ma

For the last model runs, we modify our setup: while the glacial index function is kept, the initial topography is set to a peneplain (around 1200 m elevation), mimicking the pre-rift phase of the western branch of the EARS, and then the onset of uplift at around 2 Ma of the Rwenzori Mountains (e.g. Burke and Gunnell 2008, and references therein). As discussed above, the exact timing of disruption of this quasi peneplain by extreme uplift of the Rwenzori fault block is not well constrained so far and the model run must be considered as a simplified end-member approach.

We now define an area enclosed by the Bwamba fault in the west, and the Rwimi-Wasa fault and the Nyamwamba fault in the east (Fig. 2). The area within these normal faults uplifts with a constant rock uplift rate U (mm year^{-1}), while the area outside keeps its elevation. With this setup, we mimick the rapid uplift of the Rwenzori horst.

For the morphological processes, we fixed the parameter values to $\kappa_D = 0.5$ m^2 year^{-1} for hillslope diffusion, $\kappa_R = 0.02$ for fluvial erosion, and $\kappa_G = 0.01$ for glacial abrasion. When compared to the two previous sections, we have reduced the effect of hillslope diffusion and increased the strength of fluvial erosion. The reason for these changes stems from the time frame considered: as we allow the block to uplift for 2 Ma, and the resulting morphology should be reminiscent of the real Rwenzori Mountains, an increase in fluvial erosion is needed. Again, this demonstrates the offset between landscape degradation by diffusion, erosion, and abrasion on the one hand and rock uplift on the other hand: the fixed time frame needs a rock uplift rate between 1.5 and 2 mm year^{-1} to reach the height of the present-day Rwenzori Mountains; thus, more intense erosion is needed.

Setup3 Four snapshots of the evolving block are shown in Fig. 7, showing both topography and possible ice cover.

For the early phase (1.6 Ma BP), the block bounded by the faults starts uplifting. As the surface of the block is fairly flat (peneplain assumption), water runs off evenly, and no channelling occurs. The edges of the block are subject to erosion; in fact, the hillslope diffusion smoothes the edges of the block (strong second derivative), while runoff

along the steep edges causes incision of steep channels by fluvial erosion. The low elevation of the uplifted block forbids glaciation at this stage.

Further into the model time (800 ka BP), the block has uplifted further, and the steep channels draining the interior of the block have further incised. Along the eastern edge, one channel has captured a larger upstream area of the block, and a drainage system has started developing in the central part of the block.

The next time step (20 ka BP) is the LGM. The block has already reached a height of around 4000 m to become glaciated during colder glacial periods, and a substantial ice cap covers the entire high-mountain part of the Rwenzori block. Thus, glacial abrasion has started contributing to the degradation of the block.

The final snapshot (0 ka BP) represents the present-day situation: the block has evolved to around 5 km maximum height, but under interglacial conditions there is no ice cover during that time. The flat surface of the initial block has been dissected completely by fluvial erosion, and a large deep valley drains large parts of the eastern side. Although this final topography is a completely synthetic one, it resembles the shape of the Rwenzori Mountains. Osmaston (1989) confirms from geomorphological studies that palaeosurfaces in the Rwenzoris are hardly conserved and the present relief is a combination of fluvial downcutting and glacial scouring. Thus, we can argue that we have captured, to first order, the main processes relevant for shaping the Rwenzori. Young differential uplift of individual blocks is not sufficiently constrained and quantitatively known from thermochronological data to be considered in our model runs over the last 2 Ma.

In Fig. 8a, the ice cover as a function of time is shown for the model runs with rock uplift rates of $U = 1.5$, $U = 1.6$, and $U = 1.8$ mm year^{-1} (black areas, solid red line, and dashed red line, respectively), and additionally the ice cover of the 800-Ma run with ice-sheet evolution, morphological processes, and rock uplift from setup1c (blue areas) is shown. The curves are only plotted for the last 800 ka, because glaciation for all evolving peneplain models starts not before that time. To achieve the observed glacial cover especially for the older glaciations, a sufficiently large rate above 1.6 mm year^{-1} needs to be considered over the 2 Ma of evolution, as only uplift rates above this threshold result in the area needed for substantial glaciation.

In Fig. 8b, the removal rates as a function of time are shown for the block uplift model with an average rock uplift rate of $U = 1.8$ mm year^{-1}. Here, both maximum rates for fluvial erosion and hillslope diffusion (solid red and black lines) show a distinctively different behaviour than before: after an initial phase, these two rates stagnate around 1 mm year^{-1} and increase suddenly about one order of magnitude at about 1 Ma. This increase is caused by a catchment capture of the single ravine on the eastern side, which causes a reorganisation of the drainage network and thus focusses flow into the new catchment, increasing there fluvial erosion and hillslope diffusion. The average removal rates behave much smoother, as they increase slowly and approach an almost constant value from 1 Ma BP onwards. Glacial abrasion starts at around 650 ka BP, when the uplifted block passes the elevation of the equilibrium line in its centre. The glacial abrasion rate then increases by one order of magnitude for younger glacial cycles, as the block gains further elevation. Note the drop in the average fluvial erosion rate during the peak glacial phases, because the high-mountain area is glaciated and less water is available for fluvial erosion. The maximum fluvial erosion rates peak shortly after the peak glacial phases, as the glacial sediments are transported out during melting of the ice cap.

Comparison of scenarios

From the modelled topographic data, we have derived a hypsometric distribution of elevations (Fig. 9). In Fig. 9a, the dark grey bars indicate the initial topography for setup1 and setup2, which is a smoothed version of the real topography derived from the SRTM-data. The distribution has a clear maximum at around 1000 m altitude, reflecting the local base level for the fluvial erosion of the Rwenzori Mountains. Between the present and the LGM snowlines, no clear second maximum is present. Following Egholm et al. (2009), this indicates no pronounced glacial influence; otherwise, a local glacial base level should be present just below the present snowline. However, the steepness of the terrain in the Rwenzori Mountains restricts the glaciated area substantially and a pronounced glacial effect is not expected due to the limited area available for glacial abrasion.

The modelled topographies for setup1 are shown as coloured lines at the end of the run time (0 ka BP). For setup1a (only ice-sheet evolution), of course no change is observed, as there is no ice in the model at present (red line). For setup1b (ice-sheet evolution, morphological processes), a slight change in the distribution can be observed (green line): the degradation of the landscape by fluvial erosion and hillslope diffusion results in less elevation in the high-mountain areas (≈4500 m), while sediments have been deposited along the foothills (≈1500 m). For the last model setup1c (ice-sheet evolution, morphological processes, rock uplift), the distribution is almost restored to the initial topography (blue line), just the sediment cover along the foothills causes a deviation.

The modelled topographies for setup3, the model starting from a peneplain topography, are distinctively different (Fig. 9b): starting from a uniform distribution (dark grey bar), all models at present (0 ka BP) mimick the

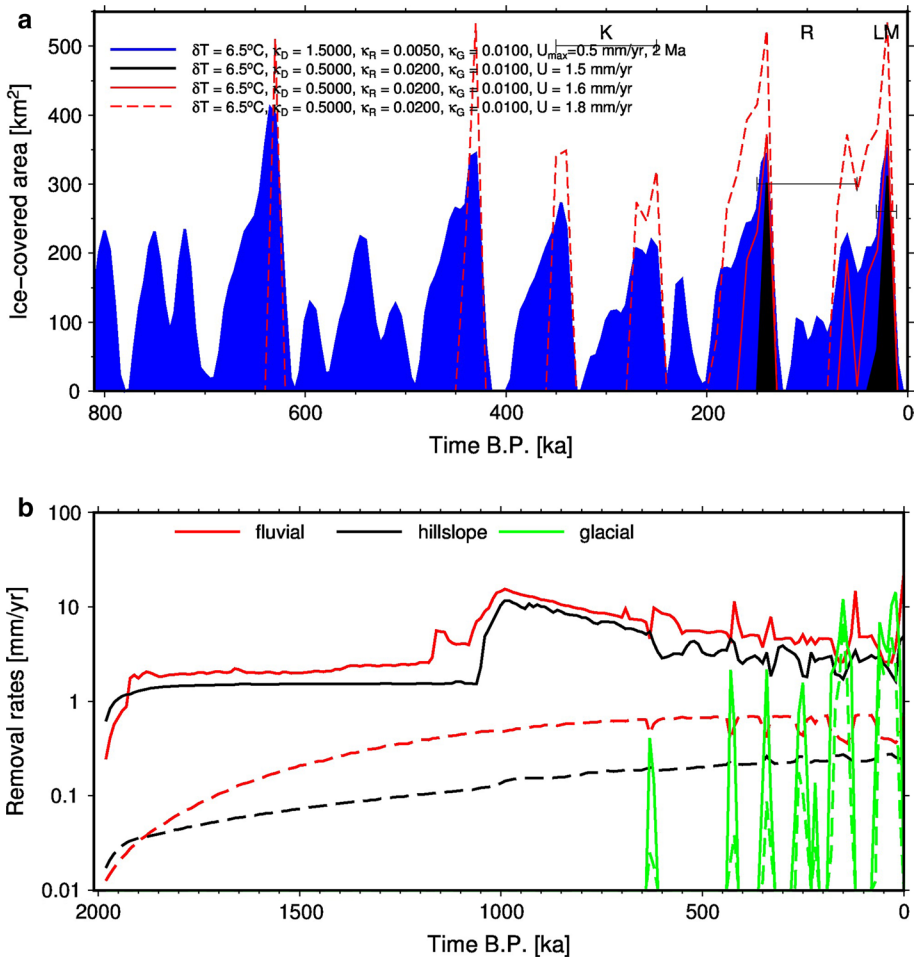

Fig. 8 Setup 3: **a** ice-covered area as a function of time BP. Lines resp. *coloured areas* represent runs with different parameters (see text). Also shown are the observed moraine-covered areas for the three different glaciations Katabarua (K), Rwimi (R), and Lake Mahoma (LM). **b** Removal rates for different processes (see legend). *Solid lines* indicate maximum rates, *dashed lines* average rates

steep slopes of the Rwenzori Mountains (light grey bars) within the altitude range 2000–3500 m, but deviate along the highest parts of the mountains. The missing topography in 1500 m elevation results from the peneplain assumption, which neglects the rift topography present in nature (light grey bars).

Discussion

The Rwenzori Mountains are the highest non-volcanic elevation of the African continent, situated in the western branch of the East African Rift system (EARS). The high altitude of the mountain chain, which experienced several glacial phases during the last couple of 100 ka, is challenging to explain within the context of the extensional setting of the EARS.

We have presented numerical simulations of the evolution of the Rwenzori Mountains, based on the landscape evolution model ULTIMA THULE. The outcome of this modelling study can be highlighted by three main questions and answers:

1. *Is the numerical evolution, which is driven by a glacial index function to simulate glacial cycles, strongly dependent on the choice of the palaeoarchive (Antarctic ice core or marine isotope records) used for the glacial index function?* Our results show that the dependence is only weak. We have compared the model runs driven by the scaled stack of marine oxygen-isotope records derived from benthic foraminifera (Lisiecki and Raymo 2005) with results from an older study (Kaufmann and Romanov 2012), where the evolution was driven by the scaled hydrogen-isotope record of the Dome C Antarctic ice core (Petit et al. 1999). Despite the different origins of both index functions, the results are remarkably stable and almost independent of the archive used, as long as the glacial cyclicity is present.
2. *How dependent is a quasi-steady state in the model on the time period considered?* We could show that an extension of the simulation from 800 ka to 2 Ma does not change the general landscape pattern and the varying contributions from fluvial erosion, hillslope diffusion, and glacial abrasion, when they are balanced by

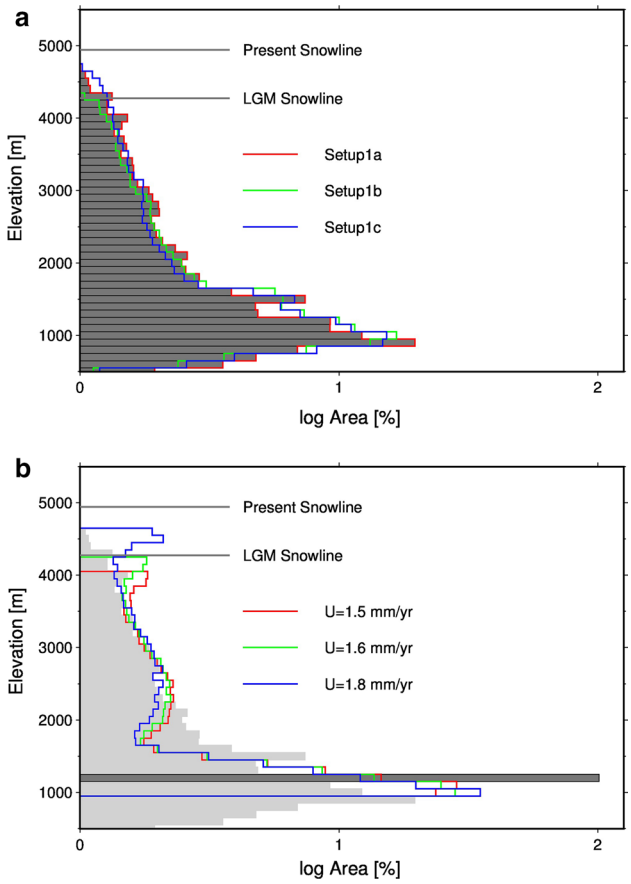

Fig. 9 Hypsometric distribution of topography. **a** Observed present-day topography distribution (*dark grey bars*), modelled topography distribution at present for setup1a (*red line*), for setup1b (*green line*), for setup1c (*blue line*). **b** Observed present-day topography distribution (*light grey bars*), modelled topography distribution at 2 Ma (peneplain) for setup3 (*dark grey bar*), at present for setup3 and $U = 1.5$ mm year^{-1} (*red line*), at present for setup3 and $U = 1.6$ mm year^{-1} (*green line*), at present for setup3 and $U = 1.8$ mm year^{-1} (*blue line*)

a rock uplift rate. There is, however, an offset between rock uplift rate and the strength of the morphological processes considered, and higher rock uplift rates require stronger degradation of the landscape induced by more pronounced fluvial erosion, hillslope diffusion, and glacial abrasion.

3. *Does the numerical model starting from a peneplain as suggested in* Burke and Gunnell (2008) *evolve to a Rwenzori-style mountain block within 2 Ma?* We were able to reproduce a typical "Rwenzori-style" mountain chain from a peneplain, which began uplifting 2 Ma ago along the prominent faults surrounding the block. The shape of the evolved landscape, with steep valleys controlled by fluvial incision and glacial landforms at higher elevations, resembles well the present topography of the Rwenzori Mountains.

Our numerical models have thus been successful in unravelling the interplay between active tectonics, isostasy, and erosional degradation of the Rwenzori Mountains. Several key aspects can be derived from our different scenarios:

- The dominant process shaping the landscape of the Rwenzori Mountains is fluvial erosion. As there is plenty of water available and the mountains are wet almost the entire year, material removed from bedrocks by fluvial erosion constantly causes incision of the steep valleys. Average erosion rates are around 0.1–1 mm year^{-1}, with only minor variations due to the climatic fluctuations. The magnitude of these rates corresponds well to those measured by terrigenous cosmogenic nuclides in modern rivers (Roller et al. 2012). Peak fluvial erosion rates are almost one order of magnitude higher and can reach 10 mm year^{-1} removal; here, the climate variability between glacial and interglacial phases has a more pronounced effect.

- Redistribution of material by hillslope processes is also important, and both the average and the peak removal rates for this diffusive process keep pace with fluvial incision. However, hillslope processes depend entirely on the soft material provided by fluvial erosion and thus only redistributes eroded material.

- Glacial abrasion has the largest variability once it became cold enough to provide a substantial ice cover after 500 ka BP. Here, both the average and peak removal rates are similar. However, the total effect on landscape degradation for glacial abrasion is limited to the highest peaks of the Rwenzori Mountains; thus, the total contribution to the degradation of the landscape is small when compared to fluvial erosion and hillslope diffusion.
- To maintain its high elevation, the Rwenzori Mountains need to be actively uplifted with an average long-term rate of around 1–2 mm year^{-1}. We derive this value from the evolution of the peneplain existing around 2 Ma ago to a high-mountain area at present within these 2 Ma. To obtain a landscape morphology similar to the real Rwenzori Mountains, the fairly strong fluvial incision component needs to be balanced by rock uplift to maintain the present high altitude needed for repeated glaciations during the last glacial cycles.
- Glacial abrasion starts to become relevant at around 500 ka BP, when the top of the Rwenzori block passed the equilibrium line altitude (ELA). The glacial abrasion then keeps the top part of the Rwenzori Mountains at its present elevation. This effect, termed *glacial buzzsaw*, has been shown to control the peak elevation

of an uplifting landscape due to the feedback between uplift beyond the ELA and glacial incision reducing the altitude again (e.g. Tomkin 2007, 2009; Egholm et al. 2009).

- Landscape evolution models including ice coverage and related glacial abrasion processes are relatively new (e.g. Braun et al. 1999; Tomkin and Braun 2002). Several regional modelling studies, e.g. for the Chugach-St. Elias Range, Alaska (Spotila et al. 2004), for the Sierra Nevada, USA (Kessler et al. 2006), and for the Southern Alps, New Zealand (Tomkin 2007; Herman and Braun 2008; Tomkin 2009), have revealed a complex interplay between rock uplift and erosional processes, resulting in transient landforms, when the region has been glaciated substantially and then reverts to fluvial erosion. In our scenarios, we can confirm the complex interplay between the different processes, especially the correlation between the strength of fluvial incision and rock uplift rate. However, the area affected by glacial processes in our scenarios for the evolution of the Rwenzori Mountains is limited to the high alpine area.
- We did not explicitly consider the effect of reduced precipitation during some cold spells as indicated by regional palaeoclimate reconstructions (e.g. Beuning et al. 1997; Bonnefille and Chalie 2000; Felton et al. 2007; Trauth et al. 2003). However, we can speculate that the temperature is at first responsible for providing areas above the ELA to initiate glaciation. If an ice cover is initiated its extent of course depends on the precipitation available. Thus, a reduced precipitation as suggested for the period 30–23 ka BP would result in less ice cover as our model suggest, and thus, glacial abrasion would be slightly reduced. In addition, there are no indications of an ice cap on the Rwenzori Mountains at MIS 6, although this is the case in our model. Probably, missing evidences are due to extremely dry intervals at this time. On the other hand, it cannot be excluded that remains of such a glaciation were completely overprinted by the subsequent Lake Mahoma Stage.

Conclusions

We have modelled the evolution of the Rwenzori Mountains with the numerical landscape evolution model ULTIMA THULE. The modelled landscape evolves from a peneplain 2 Ma ago to a Rwenzori-type mountain range, when the fairly strong average rock uplift rate of 1–2 mm year^{-1} is compensated by a strong fluvial erosion component. A rock uplift rate of 1–2 mm ka^{-1} is needed to compensate for erosion and rise the topography by about 3500 m within 2 Ma and to obtain elevations above the equilibrium line altitude of glaciation at around 500 ka. Around that time, a periodic ice cap appears in the model runs, and glacial abrasion then limits the height of the Rwenzori Mountains to its present elevation, concordant to the hypothesis of glacial buzzsaw acting at high-mountain ranges.

Acknowledgments We thank Friederike Bauer and another anonymous reviewer for their thorough reviews which helped improving the manuscript. The authors acknowledge the support by the Deutsche Forschungsgemeinschaft (DFG) under the Research Group RIFTLINK (FOR 703, Rift Dynamics, Uplift and Climate Change in Equatorial Africa: Interdisciplinary Research linking Asthenosphere, Lithosphere, Biosphere and Atmosphere). Within the RIFTLINK framework, DR has been funded by the DFG under research Grant KA1723/7, MH under research Grant HI643/7-2. Figures were prepared using GMT software (Wessel and Smith 1998).

References

Barker PA, Hurrell ER, Leng MJ, Wolff C, Cocquyt C, Sloane HJ, Verschuren D (2011) Seasonality in equatorial climate over the past 25 ky revealed by oxygen isotope records from Mount Kilimanjaro. Geology 39(12):1111–1114

Bauer FU, Glasmacher UA, Ring U, Schumann A, Nagudi B (2010) Thermal and exhumation history of the central Rwenzori Mountains, Western Rift of the East African Rift System, Uganda. Int J Earth Sci 99(7):1575–1597

Bauer FU, Karl M, Glasmacher UA, Nagudi B, Mroszewski L (2012) The Rwenzori Mountains of western Uganda—aspects on the evolution of their remarkable morphology within the Albertine Rift. J Afr Earth Sci 73–74:44–56

Bauer FU, Glasmacher UA, Ring U, Karl M, Schumann A, Nagudi B (2013) Tracing the exhumation history of the Rwenzori Mountains, Albertine Rift, Uganda, using low-temperature thermochronology. Tectonophysics 599:8–28. doi:10.1016/j.tecto.2013.03.032

Beaumont C, Fullsack P, Hamilton J (1992) Erosional control of active compressional orogens. In: McClay KR (ed) Thrust tectonics. Chapman and Hall, New York, pp 1–18

Beuning KRM, Talbot MR, Kelts K (1997) A revised 30,000-year paleoclimatic and paleohydrologic history of Lake Albert, East Africa. Palaeogeogr Palaeoclimatol Palaeoecol 136:259–279

Bonnefille R, Chalie F (2000) Pollen-inferred precipitation time-series from equatorial mountains, Africa, the last 40 kyr BP. Glob Planet Change 26:25–50

Braun J, Sambridge M (1997) Modelling landscape evolution on geological time scales: a new method based on irregular spatial discretisation. Basin Res 9:27–52

Braun J, Willet SD (2013) A very efficient $o(n)$, implicit and parallel method to solve the stream power equation governing fluvial incision and landscape evolution. Geomorphology 180181:170179

Braun J, Zwartz D, Tomkin JH (1999) A new surface processes model combining glacial and fluvial erosion. Ann Glaciol 28:282–290

Burke K, Gunnell Y (2008) The African erosion surface: a continental-scale synthesis of geomorphology, tectonics, and environmental change over the past 180 million years, vol 201. Geological Society of America Memoir

Ebinger CJ (1989) Tectonic development of the western branch of the East African rift system. Geol Soc Am Bull 101:885–903

Ebinger CJ, Sleep NH (1998) Cenozoic magmatism throughout East Africa resulting from impact of a single plume. Nature 395:788791

Egholm DL, Nielsen SB, Pedersen VK, Lesemann J-E (2009) Glacial effects limiting mountain height. Nature 460:884–888
EPICA (2004) Eight glacial cycles from an Antarctic ice core. Nature 429:623–628
Farr TG, Rosen PA, Caro E, Crippen R, Duren R, Hensley S, Kobrick M, Paller M, Rodriguez E, Roth L, Seal D, Shaffer S, Shimada J, Umland J, Werner M, Oskin M, Burbank D, Alsdorf D (2007) The shuttle radar topography mission. Rev Geophys 45:RG2004. doi:10.1029/2005RG000183
Felton AA, Russell JM, Cohen Andrew S, Baker Mark E, Chesley John T, Lezzar Kiram E, McGlue Michael M, Pigati Jeffrey S, Jay Quade, Curt Stager J, Jacques Tiercelin Jean (2007) Paleolimnological evidence for the onset and termination of glacial aridity from lake Tanganyika, Tropical East Africa. Palaeogeogr Palaeoclimatol Palaeoecol 252:405–423
Foley S, Link K, Tiberindwa JV, Barifajio E (2012) Patterns and origin of igneous activity around the Tanzanian craton. J Afr Earth Sci 62:1–18
Gasse F (2000) Hydrological changes in the African tropics since the last glacial maximum. Quat Sci Rev 19:189–211
Hallet B (1979) A theoretical model of glacial abrasion. J Glaciol 17:209–222
Herman F, Braun J (2008) Evolution of the glacial landscape of the Southern Alps of New Zealand: insights from a glacial erosion model. J Geophys Res 113:F02009. doi:10.1029/2007JF000807
Hutter K (1983) Theoretical glaciology. Riedel, Dortrecht
Jarvis A, Reuter HI, Nelson A, Guevara E (2008) Hole-filled seamless SRTM data V4. International Centre for Tropical Agriculture (CIAT). http://srtm.csi.cgiar.org
Kapelle M (2004) Encyclopedia of forest sciences, chapter tropical montane forests. Elsevier, Oxford, pp 1782–1792. doi:10.1016/B0-12-145160-7/00175-7
Kaser G (2001) Glacier-climate interaction at low latitudes. J Glaciol 47(157):195–204
Kaspar F, Prmmel K, Cubasch U (2010) Impacts of tectonic and orbital forcing on East African climate: a comparison based on global climate model simulations. Int J Earth Sci 99(7):1677–1686
Kaufmann G (2010) ULTIMA THULE: a numerical landscape evolution model. User guide version 1.0
Kaufmann Georg, Romanov Douchko (2012) Landscape evolution and glaciation of the rwenzori mountains: insights from numerical modelling. Geomorphology 138:263–275
Kessler M, Anderson R, Stock G (2006) Modeling topographic and climatic control of east–west asymmetry in Sierra Nevada glacier length during the last glacial maximum. J Geophys Res 111:F02002. doi:10.1029/2005JF000365
Koehn D, Lindenfeld M, Rümpker G, Aanyu K, Haines S, Passchier CW, Sachau T (2010) Active transsection faults in rift transfer zones: evidence for complex stress fields and implications for crustal fragmentation processes in the western branch of the East African Rift. Int J Earth Sci 99(7):1633–1642
Kooi H, Beaumont C (1994) Escarpment evolution on high-elevation rifted margins: insights derived from a surface processes model that combines diffusion, advection, and reaction. J Geophys Res 99(B6):12191–12209
Lindenfeld M, Rümpker G, Batte A, Schumann A (2012) Seismicity from February 2006 to September 2007 at the Rwenzori Mountains, East African Rift: earthquake distribution, magnitudes and source mechanisms. Solid Earth 3:1–14
Link K, Koehn D, Barth MG, Tiberindwa JV, Barifaijo E, Aanyu K, Foley SF (2010) Continuous cratonic crust between the Congo and Tanzania blocks in western Uganda. Int J Earth Sci 99(7):1559–1573
Lisiecki LE, Raymo ME (2005) A pliocene–pleistocene stack of 57 globally distributed benthic d18O records. Paleoceanography 20:PA1003. doi:10.1029/2004PA001071
Morley CK (1999) Tectonic evolution of the East African Rift System and the modifying influence of magmatism: a review. Acta Vulcanol 11(1):119
Osmaston HA (1989) Glaciers, glaciations, and equilibrium line altitudes on the Rwenzori. Quat Environ Res East Afr Mt 1:31–104
Osmaston HA, Harrison SP (2005) The late quaternary glaciation of Africa: a regional synthesis. Quat Int 138–139:32–54
Petit JR, Jouzel J, Raynaud D, Barkov NI, Barnola J-M, Basile I, Bender M, Chappellaz J, Davis M, Delaygue G, Delmotte M, Kotlyakov VM, Legrand M, Lipenkov VY, Lorius C, Pepin L, Ritz C, Saltzman E, Stievenard M (1999) Climate and atmospheric history of the past 420,000 years from the Vostok ice core, Antarctica. Nature 399:429–436
Pickford M (1990) Uplift of the roof of Africa and its bearing on the evolution of mankind. Hum Evol 5(1):1–20
Pickford M, Senut B, Hadoto D (1993) Geology and palaeontology of the Albertine Rift Valley, Uganda-Zaire, vol 24. Publication Occasionelle, Centre International pour la Formation et les Echanges Geologiques, Orleans Cedex 2
Prömmel K, Cubasch U, Kaspar F (2013) A regional climate model study of the impact of tectonic and orbital forcing on African precipitation and vegetation. Palaeogeogr Palaeoclimatol Palaeoecol 369:154–162
Ring U (1993) Aspects of the kinematic history and mechanisms of superposition of Proterozoic mobile belt of eastern Central Africa (northern Malawi and southern Tanzania). Precambrian Res 62:207–226
Ring U (2008) Extreme uplift of the Rwenzori Mountains in the East African Rift, Uganda: structural framework and possible role of glaciations. Tectonics 27. doi:10.1029/2007TC002176
Ritsema J, Ni S, Helmberger DV, Crotwell HP (1999) Evidence for strong shear velocity reduction and velocity gradients in the lower mantle beneath Africa. Geophys Res Lett 25:4245–4248
Roller S, Hornung J, Hinderer M, Ssemmanda I (2010) Middle miocene to pleistocene sedimentary record of rift evolution in the southern Albert Rift (Uganda). Int J Earth Sci 99(7):1643–1661
Roller S, Wittmann H, Kastowski M, Hinderer M (2012) Erosion of the Rwenzori Mountains, East African Rift, from in situ-produced cosmogenic ^{10}Be. J Geophys Res 117:F03003. doi:10.1029/2011JF002117
Sachau T, Koehn D (2010) Faulting of the lithosphere during extension and related rift-flank uplift: a numerical study. Int J Earth Sci 99(7):1619–1632
Sachau T, Koehn D, Passchier C (2013) Mountain-building under extension. Am J Sci 313:326–344. doi:10.2475/04.2013.03
Scholz CA, Johnson TC, Cohend AS, Kinge JW, Peck JA, Overpeck JT, Talbot MR, Brown ET, Kalindekafeh L, Philip YOA, Robert PL, Timothy MS, Isla SC, Clifford WH, Steven LF, Lanny RM, Kristina RB, Jeanette G, James P (2007) East African megadroughts between 135 and 75 thousand years ago and bearing on early-modern human origins. PNAS 104(42):16416–16421
Shanahan T, Zreda M (2000) Chronology of quaternary glaciations in East Africa. Earth Planet Sci Lett 177:23–42
Spotila JA, Busher JT, Meigs AJ, Reiners PW (2004) Longterm glacial erosion of active mountain belts: example of the chugach-St. Elias Range, Alaska. Geology 32:501–504
Taylor RG, Mileham L, Tindimugaya C, Majugu A, Muwanga A, Nakileza B (2006) Recent glacial recession in the Rwenzori Mountains of East Africa due to rising air temperature. Geophys Res Lett 33. doi:10.1026/2006GL025962
Tomkin J (2003) Feedbacks and the oscillation of ice masses. J Geophys Res 108(B10). doi:10.1029/2002JB002087
Tomkin J (2007) Coupling glacial erosion and tectonics at active orogens: a numerical modeling study. J Geophys Res 112:F02015. doi:10.1029/2005JF000332

Tomkin JH, Braun J (2002) The influence of alpine glaciation on the relief of tectonically active mountain belts. Am J Sci 302:169–190

Tomkin JH (2009) Numerically simulating alpine landscapes: the geomorphologic consequences of incorporating glacial erosion in surface process models. Geomorphology 103:180–188

Trauth MH, Deino AL, Bergner AGN, Strecker MR (2003) East African climate change and orbital forcing during the last 175 kyr BP. Earth Planet Sci Lett 206:297–313

Tucker GE, Slingerland RL (1994) Erosional dynamics, flexural isostasy, and long-lived escarpments: a numerical modeling study. J Geophys Res 99:12229–12243

Turcotte DL, Schubert G (1982) Geodynamics. Wiley, New York

Van Damme D, Pickford M (2003) The late Cenozoic Thiaridae (Mollusca, Gastropoda, Cerithioidea) of the Albertine Rift Valley (Uganda-Congo) and their bearing on the origin and evolution of the Tanganyikan thalassoid malacofauna. Hydrobiologia 498:183

van der Beek P, Bishop P (2003) Cenozoic river profile development in the Upper Lachlan catchment (SE Australia) as a test of quantitative fluvial incision models. J Geophys Res 108:2309. doi:10.1029/2002JB002125

Wallner H, Schmeling H (2010) Rift induced delamination of mantle lithosphere and crustal uplift: a new mechanism for explaining Rwenzori Mountains extreme elevation? Int J Earth Sci 99(7):1511–1524

Wallner H, Schmeling H (2011) Sensitivity analysis of rift induced delamination with application to Rwenzori Mountains. Geophys J Int 187:1135–1145

Wessel P, Smith WHF (1998) New, improved version of generic mapping tools released. EOS 79:579

Wölbern I, Rümpker G, Schumann A, Muwanga A (2010) Crustal thinning beneath the Rwenzori region, Albertine Rift, Uganda, from receiver-function analysis. Int J Earth Sci 99(7):1545–1557